

Bootstrapping non-unitary CFTs

Yu-tin Huang^{1, 2, 3, *} Shao-Cheng Lee^{1, †} Henry Liao^{1, ‡} and Justinas Rumbutis^{1, 4}

¹*Department of Physics and Center for Theoretical Physics,
National Taiwan University, Taipei 10617, Taiwan*

²*Physics Division, National Center for Theoretical Sciences, Taipei 10617, Taiwan*

³*Max Planck-IAS-NTU Center for Particle Physics,
Cosmology and Geometry, Taipei 10617, Taiwan*

⁴*Institute for Mathematics, Academia Sinica, Taiwan*[§]

In this letter, we present an evolutionary algorithm-based approach to bootstrapping the spectrum of general conformal field theories (CFTs). Starting from a trial spectrum, we invert the crossing equations to extract the corresponding operator product expansion (OPE) coefficients. The statistical distribution of these coefficients, obtained by sampling over cross-ratios, provides a quantitative measure of how closely crossing symmetry is satisfied. We then define a reward function based on this statistic and employ a genetic algorithm to search for spectra that maximize the reward. A key advantage of our framework is that it does not rely on unitarity. We illustrate the method using Virasoro blocks with central charge $c < 1$, where the optimal solutions align with the known minimal models. More broadly, this approach - solving systems of nonlinear constraints by exploiting the statistical properties of associated linear variables - provides a general strategy for broad class of bootstrap problems.

I. INTRODUCTION

Since the seminal work of Rattazzi, Rychkov, Tonni, and Vichi [1], which introduced the modern numerical framework for the conformal bootstrap [2] - casting crossing symmetry and unitarity as a convex optimization problem and thereby obtaining rigorous bounds on operator dimensions - there has been remarkable progress in constraining the operator spectrum and critical exponents of CFTs across various spacetime dimensions. (see [3] for comprehensive review)

The numerical bootstrap program faces two main challenges. First, casting the CFT bootstrap as an optimization problem naturally maps out the boundary of “theory space” in the space of CFT data. This framework yields powerful constraints when notable theories lie along the boundary, or form isolated “islands” once additional assumptions are imposed—as in the celebrated cases of the 3D Ising and O(N) models [4–6]. Nevertheless, it is highly desirable to explore where inside the theory space do physical theories populate. Second, the reformulation of the bootstrap as an optimization problem relies critically on unitarity. Yet nonunitary CFTs are of considerable interest, appearing in contexts such as RG flows near complex fixed points and holography in more general backgrounds.

To find explicit solutions, even approximately, to the bootstrap equations [7], one must contend with the challenge of exploring a high-dimensional search space - encompassing conformal dimensions, spins, and OPE coefficients - while satisfying an infinite set of constraints,

namely, the vanishing of crossing violations for all values of the conformal cross-ratios. Previous attempts, such as Monte Carlo methods [8] and machine - learning approaches [9–11], have achieved progress primarily when the search is restricted to a window near known theories.

In this letter, we present a novel strategy that turns these two challenges to our advantage. Given a candidate spectrum that solves the crossing equations, one can invert the constraints to determine the corresponding OPE coefficients. For an approximate spectrum, this inversion yields cross-ratio - dependent variations in the extracted OPE coefficients. The resulting distribution of OPE coefficients over different cross-ratios then provides a quantitative measure of proximity to an exact solution. In this way, the dimensionality of the search space is reduced, while the number of crossing constraints becomes a tunable parameter controlling the statistical quality of the test. This allows us to cast the bootstrap problem into a single objective maximization problem, which can be solved using various numerical approaches.

* yutin@phys.ntu.edu.tw

† ken6020255@gmail.com;

‡ henryliao.physics@gmail.com

§ jr3918@as.edu.tw

As a proof of concept, we employ covariant matrix adaptation evolution strategy (CMA-ES) [12]. For an introduction of CMA-ES as well as the spec for our searches see Appendix C. We illustrate the utility of this method in two-dimensional CFTs, where we solve the bootstrap equation for four scalar primaries, with up to 5 internal states. This represents a 7-dimensional search space. We demonstrate that our algorithm reliably recovers the first three state in the spectrum of known theories, both unitarity and non-unitary.

II. THE OBJECTIVE FUNCTION

We consider the four-point function of identical scalar primaries ϕ of scaling dimension Δ_ϕ :

$$\langle \phi(x_1)\phi(x_2)\phi(x_3)\phi(x_4) \rangle = \frac{\mathcal{G}(z, \bar{z})}{x_{12}^{2\Delta_\phi} x_{34}^{2\Delta_\phi}}, \quad (1)$$

with conformal cross-ratios $\frac{x_{12}^2 x_{34}^2}{x_{13}^2 x_{24}^2} = z\bar{z}$, $\frac{x_{14}^2 x_{23}^2}{x_{13}^2 x_{24}^2} = (1-z)(1-\bar{z})$. The reduced correlator admits the s -channel conformal block expansion [13, 14]

$$\mathcal{G}(z, \bar{z}) = \sum_{\mathcal{O}} (f_{\phi\phi\mathcal{O}})^2 g_{\Delta_{\mathcal{O}}, s_{\mathcal{O}}}^{\Delta_\phi}(z, \bar{z}), \quad (2)$$

where $f_{\phi\phi\mathcal{O}}$ are the OPE coefficients and $g_{\Delta_{\mathcal{O}}, s_{\mathcal{O}}}^{\Delta_\phi}(z, \bar{z})$ are the (scalar-external) conformal blocks. The equivalence of s - and t -channel OPE expansion leads to the crossing equation:

$$\sum_{k=1} (f_{\phi\phi k})^2 G_{\Delta_k, s_k}^{\Delta_\phi}(z, \bar{z}) = vac(z, \bar{z}), \quad (3)$$

where $G_{\Delta_k, s_k}^{\Delta_\phi}$ is the difference of the s and t channel conformal blocks and $vac(z, \bar{z})$ is the vacuum contribution.

As we will be searching in finite dimensional space, we will be solving the crossing equation with only finite set of spectrum. Therefore it is more fitting to write eq.(3) as:

$$\sum_{k=1}^N (f_{\phi\phi k})^2 G_{\Delta_k, s_k}^{\Delta_\phi}(z, \bar{z}) + e(z, \bar{z}) = vac(z, \bar{z}), \quad (4)$$

where N is the number of low lying states, $e(z, \bar{z})$ represents the contributions from primaries with $\Delta_i > \Delta_N$.¹ In the vicinity of the symmetric point $z=\bar{z}=\frac{1}{2}$, the function $G_{\Delta_k, s_k}^{\Delta_\phi}$ is exponentially suppressed for large conformal dimensions [15]. Thus, we expect that for a large class of systems, if we consider points around the symmetric point, e in eq.(4) can be approximately set to zero.

With this in mind, we consider N points $\{z_j, \bar{z}_j\}$ in the vicinity of $z=\bar{z}=\frac{1}{2}$. For these points eq.(4) can be organized as:

$$\sum_{k=1}^N C_k G_{k,j} + e_j = v_j, \quad (5)$$

where $C_k = (f_{\phi\phi k})^2$, $G_{k,j} = G_{\Delta_k, s_k}^{\Delta_\phi}(z_j, \bar{z}_j)$ and $v_j = vac(z_j, \bar{z}_j)$. For every choice of the N $\{z_j, \bar{z}_j\}$ points (we

denote them as $\{z\}$) we have a matrix equation, linear in the squared OPE coefficients, \mathbf{C} :

$$G_{\{z\}} \cdot \mathbf{C} + \mathbf{e}_{\{z\}} = \mathbf{v}_{\{z\}}. \quad (6)$$

Solving the crossing equations with $\mathbf{e}_{\{z\}}$ set to zero leads to OPE coefficients that are formally z -dependent, $\mathbf{C}_{\{z\}}$,

$$\mathbf{C}_{\{z\}} = G_{\{z\}}^{-1} \cdot \mathbf{v}_{\{z\}}. \quad (7)$$

If this were the exact bootstrap equation, then the solution $\mathbf{C}_{\{z\}}$ would be in fact $\{z\}$ -independent. However, since we are working with an approximate crossing equation, $\mathbf{C}_{\{z\}}$ will depend on $\{z\}$ and their statistical distribution becomes a measure of how close one is to an exact solution. In particular, we can consider $n(\geq N)$ sets of $\{z\}$, each time inverting eq.(6), to obtain n sets of $\mathbf{C}_{\{z\}}$. By taking the standard deviation of the result, we obtain a qualitative measurement on how different z points agree on the values of the OPE coefficients. This standard deviation of the distribution over $\{z\}$ points, which we denote σ_z , is related to the error term, $\mathbf{e}_{\{z\}}$, which we have ignored, since

$$\begin{aligned} \mathbf{C}_{\{z\}} &= G_{\{z\}}^{-1} \cdot \mathbf{v}_{\{z\}} = \mathbf{C} + G_{\{z\}}^{-1} \cdot \mathbf{e}_{\{z\}}, \\ \sigma_z(\mathbf{C}_{\{z\}}) &= \sigma_z(\mathbf{C} + G_{\{z\}}^{-1} \cdot \mathbf{e}_{\{z\}}) = \sigma_z(G_{\{z\}}^{-1} \cdot \mathbf{e}_{\{z\}}), \end{aligned} \quad (8)$$

where \mathbf{C} is the OPE coefficient of the truncated spectrum and independent of $\{z\}$. We see that the standard deviation of the OPE solutions of the truncated crossing equation, $\sigma_z(\mathbf{C}_{\{z\}})$, measures the contribution of the error term.

In practice since $\{z\}$ is distributed in a small neighborhood, the $N \times N$ matrix $G_{\{z\}}$ can become singular and inversion is numerically unstable. To this end we instead sample over $N_z \gg N$ number of points and solve for $\mathbf{C}_{\{z\}}$ as the least squares solution. We then consider the following objective function:

$$R = - \sum_{i=1}^{N_r} \log \left(\left| \frac{\sigma(C_{i\{z\}})}{\text{Mean}(C_{i\{z\}})} \right| \right), \quad (9)$$

where $\sigma(C_{i\{z\}})$ is the standard deviation of the solution of the OPE coefficient for the i -th state and N_r denotes the number of low-lying states whose inferred OPE coefficients are included in the objective. However, when we compare searches with different assumed numbers of internal operators, we will mostly use $N_r = 1$ and focus on the lowest-dimension state. In that case the reward is directly comparable across spectra with different numbers of internal operators.

For theories where the truncation is a good approximation the reward will be large. As we sample over N_z points, the typical relative error (due to statistical fluctuations) of $\sigma(C_{i\{z\}})$ and $\text{Mean}(C_{i\{z\}})$ is $\frac{1}{\sqrt{N_z}}$ [16]. Therefore, we expect that this objective function has an associated noise of size $O(1/\sqrt{N_z})$.

¹In practice, there will also be errors coming from the approximation for Virasoro blocks.

This allows us to instead of scanning through $\{\Delta_k, s_k, (f_{\phi\phi k})^2\}$, as done in for example [10], we only search in the space of $\{\Delta_k, s_k\}$.

III. THE 2D PROBLEM

While our setup is general, in this work we will test it on the scenario: 2d CFTs with only scalar operators. As benchmark we use the A-series minimal models, briefly reviewed in Appendix A. In such case the parameter space include the central charge c , conformal dimension of the external h_{ext} and internal operators h_{int} . We begin with one internal operator, which is a three-dimensional search, and gradually increase the number of internal operators. For numerical evaluation of the Virasoro blocks [2], we utilize the Zamolodchikov-type recursion relations with finite iterations.²

We perform the search in four different parameter spaces, characterized by the number of internal states that the known theories in the region contain. In the first three regions, the known theories contain one, two and three internal states respectively. The fourth is characterized by theories with five internal states.

In this work we search by iteratively increase the number of internal state. If at a given number N the found solution falls below a certain threshold, we then add an additional state and restart the search. On the other hand if we have passed the threshold, we still add another state and see if the reward is improved. If it does not and the search finds the same parameters of the first N states with the mean OPE value of the next state close to zero (or more precisely within a standard deviation to zero) we can conclude that N is sufficient. We estimate this threshold by looking at $N_r = 1$ reward in Eq.(9) for different minimal models. From the result in Fig. 1, we see that it is reasonable to set the threshold of the $N_r = 1$ reward at 10.

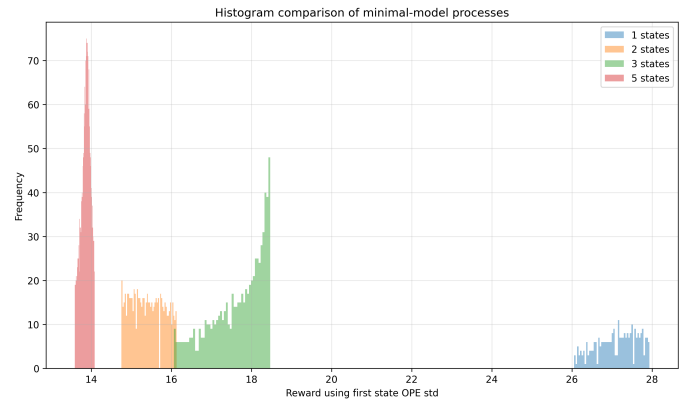


FIG. 1: The reward distributions of minimal model processes inside the four regions where we perform the search.

A. Search for exact spectra with $c < 1$ CFTs

In this part, we perform a search of CFT spectra in regions where the relevant four-point functions admit exact solutions with up to three exchanged Virasoro primaries. For these correlators we include all operators that appear in the OPE channel under consideration, so there is no truncation of the spectrum in Eq. (6). In this case the error term $\mathbf{e}_{\{z\}}$ arises solely from the numerical evaluation of Virasoro blocks, due to the finite number of recursion steps in our implementation.

Two results are presented here. The first, shown in Fig. 2, is global search of theories with a single internal operator exchange. We set the search window to be $c \in [-6, 1]$, $h_{ext} \in [-0.4, 0.6]$ and $h_{int} \in [-0.5, 1.2]$. The full search results and analytic values for minimal models align well as shown in Fig. 2.

The second one is a local search in the region where only non-unitary CFTs exist. In particular, we search in the region where $(h_{int,1}, c, h_{ext})$ are close to that of Yang-Lee CFT. The search windows are given in Table I and II. Note that the relative narrow window of search is due to the large number of minimal models and we aim to test if these models can be identified within this window. We tried to search for theories with 2 or 3 internal operators with $h_{int,1} \sim h_{YL} = -0.2$, while keeping the ascending order of \mathbf{h}_{int} ($h_{int,1} \leq h_{int,2} \leq h_{int,3}$). The results are shown in Fig. 3, which again aligns with theoretical values well. In Fig. 3, we only displayed the projections onto the plane $(h_{int,1}, c, h_{ext})$. For those related to $h_{int,2}$ and $h_{int,3}$ are given in Appendix E. Note that in principle at a given N , we should find theories with less operator exchange as well. These appear as special cases with part of the OPEs being close to 0. To prevent inefficiency for the search, we put additional penalty for small OPEs.

²We have implemented the recursive algorithm for calculating Virasoro blocks numerically of [17] on GPU. In this work we used 40 recursion iterations.

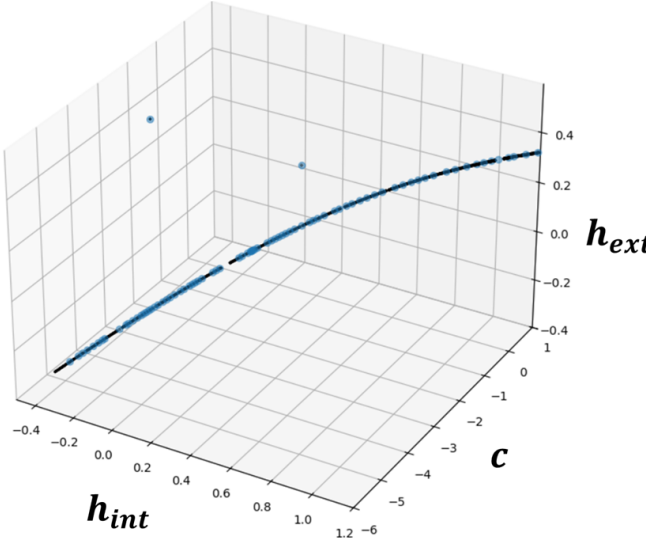


FIG. 2: Search result in $c < 1$ region with single internal operator. The blue dots are search results, while the black ones are analytic values from minimal models.

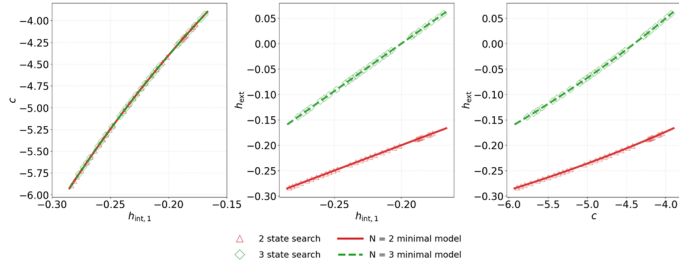


FIG. 3: Search results for non-unitary CFTs with 2 and 3 internal operators with similar $(h_{int,1}, c, h_{ext})$ as Yang-Lee CFT.

B. Result for search in truncated space with $c < 1$ CFTs

In the following, we utilize our algorithms in a region where 5 internal state processes can be found. The search window of this region is given in Table III. We start with a search of one state and keep adding more states until the search finds points above the first state reward threshold. The maximum first state reward for different N is given in Table IV, where we see that for $N < 4$ one

TABLE I: Search window for 2-state search

Variable	Search bounds
$h_{int,1}$	$[-0.3, -0.1]$
$h_{int,2}$	$[0.15, 0.5]$
c	$[-6.5, -4]$
h_{ext}	$[-0.3, -0.2]$

TABLE II: Search window for 3-state search

Variable	Search bounds
$h_{int,1}$	$[-0.3, -0.1]$
$h_{int,2}$	$[0.1, 0.5]$
$h_{int,3}$	$[1.1, 2]$
c	$[-7, -3]$
h_{ext}	$[-0.3, 0.1]$

cannot surpass the threshold of 10. Starting at $N = 4$, the threshold is passed and the points found are close to the first four states of known processes. We present five examples in Table V Appendix B. This demonstrates that our method can be used to find approximate truncated solutions. If we attempt a six state search, we find no improvement in reward compared to the exact search as indicated in Table IV. Furthermore, the mean OPE coefficient of the last state is of the same order of magnitude as its standard deviation (both around $\sim 10^{-8}$), therefore undistinguishable from zero. The other parameters for the best five and six state solutions are within 4% in relative terms, as shown in Table VI. Thus we conclude that the six state search really finds a five state with the extra state having an OPE of near zero.

TABLE III: Search window for 5-state search

Variable	Search bounds
$h_{int,1}$	$[0.23, 0.3]$
$h_{int,2}$	$[0.35, 0.4]$
$h_{int,3}$	$[1.8, 2]$
$h_{int,4}$	$[2.8, 3.2]$
$h_{int,5}$	$[6.3, 6.9]$
c	$[0.1, 0.23]$
h_{ext}	$[0.85, 0.95]$

TABLE IV: Maximum rewards of the searches with different number of states in the region given in Table III. For the best six state spectrum the mean OPE coefficient of the last state is of the same order of magnitude as its standard deviation. Therefore we conclude that the five states are sufficient to complete the spectrum.

Number of states	Max 1st state reward	$\frac{\sigma(C_{last})}{\text{Mean}(C_{last})}$
1	4.7894	4.4651×10^{-10}
2	5.3099	5.2581×10^{-10}
3	4.2433	3.2996×10^{-10}
4	12.6996	1.6291×10^{-9}
5	21.5746	6.4221×10^{-4}
6	21.5296	6.5360×10^{-1}

Next, we look at how close are the found points to the exact minimal model spectra. The 7-dimensional search region contains many minimal model spectra, so to visualize the search result in a systematic way, we plot the relative error using the procedure mentioned in Appendix D. Below, we briefly mention how it is done.

To visualize the minimal model spectra together with the search results in this seven dimensional space, for every found point we assign the closest (by Euclidean distance) minimal model spectra and calculate its relative error in every direction of the search space. Then we look at the distribution of these relative errors at the beginning and end of the search and plot their means

and standard deviations. The search results are shown in Fig. 4.

In order to see how effective the CMA-ES search is, we also plot the relative errors of the top 10% of the highest reward points at the initialization of the search. The error bars of the first four states (three in the case of three state search) are plotted with the means of corresponding relative errors and an associated error bar of length 2σ . From left to right, the colors blue, orange, green and red labels the results of random sampling (or before running the algorithm), search in space with 2 less dimension, that with 1 less dimension, and that with exact dimension with the reference theories, and they are ordered from left to right in each plot. We see that the CMA-ES search significantly reduces the relative error.

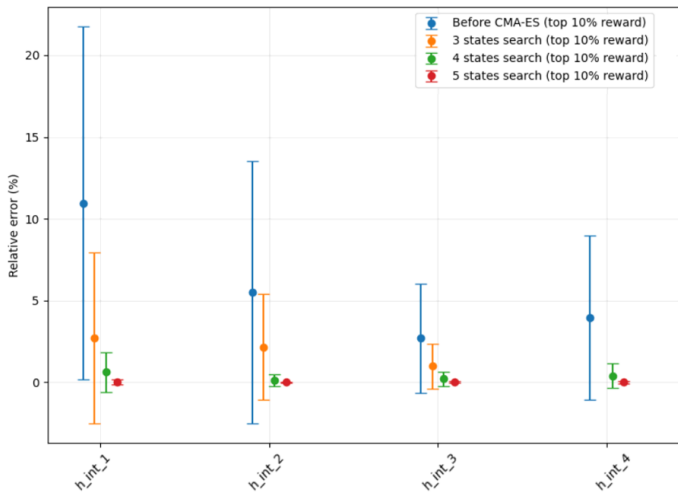


FIG. 4: Search result of different truncated space where only processes with 5 internal states are present.

IV. CONCLUSION AND OUTLOOK

In this work we proposed a simple objective function for searching CFT spectra satisfying the crossing equation, that is based on the statistics of solutions of OPE coefficients across many different z, \bar{z} points. This approach allows us to study solutions to the bootstrap equations for non-unitary CFTs, where conventional convex optimization approaches are no longer applicable. We implemented this objective function as fully GPU parallelized function [18] and demonstrated its applications in 2d CFT search for exact and truncated spectra using CMA-ES as an optimizer.

There are many immediate improvements one can implement. Firstly, we can ensure the suppression of the error term, e , in eq. (4) by constraining the contribution of states from large scaling dimensions. In particular, we can incorporate the implications of light-cone limit in $d > 2$ [19, 20], where we know the existence of double-twist operators that were hidden in e originally. Incorporating

spin and considering $d > 2$ will in general involve searches in large dimensions. This is an excellent arena to apply machine learning. In particular, since our objective is a structured (always made of conformal blocks) but non-differentiable function there might be more efficient strategies, compared to the generic optimization methods like CMA-ES, that utilize certain features of the objective function. Therefore, one could try to apply meta learning approaches [21–25] to see if a neural network could make use of some specific features of our objective functions to learn efficient optimization strategies.

Beyond non-unitary CFTs with negative scaling dimensions, central charge and squared OPE coefficients, our approach is applicable for complex CFTs, which is related to dS/CFT correspondence [26]. Also, our idea should be applicable to cases where positivity cannot be applied such as five-point bootstrap [27].

ACKNOWLEDGMENTS

We would like to thank Po-Chung Chen, Li-Yuan Chiang, Miranda Cheng, Chong-Sun Chu, David Poland and Ning Su for enlightening discussions. Y-t H thanks Riken iTHEMS and the Yukawa Institute for Theoretical Physics at Kyoto University. Discussions during “Progress of Theoretical Bootstrap” were useful in completing this work. Y-t H is supported by the Taiwan National Science and Technology Council grant 112-2628-M-002-003-MY3 and 114-2923-M-002-011-MY5. S-C Lee is supported by 112-2628-M-002-003-MY3. H Liao is supported in part by the Ministry of Science and Technology grant 112-2112-M-002-024-MY3 and 112-2628-M-002-003-MY3.

Appendix A: 2d Minimal Model CFT

In two-dimensional CFT, local primary operators are labeled by holomorphic and anti-holomorphic weights (h, \bar{h}) , with scaling dimension and spin

$$\Delta = h + \bar{h}, \quad s = h - \bar{h} \in \mathbb{Z}. \quad (\text{A1})$$

The Virasoro minimal models $M(p, q)$ are labeled by coprime integers $p > q \geq 2$, with central charge

$$c = 1 - \frac{6(p-q)^2}{pq}. \quad (\text{A2})$$

Primary fields are indexed by Kac labels (r, s) with $1 \leq r \leq q-1$ and $1 \leq s \leq p-1$, modulo the identification

$$(r, s) \sim (q-r, p-s). \quad (\text{A3})$$

Their conformal weights are

$$h_{r,s} = \frac{(pr - qs)^2 - (p-q)^2}{4pq}. \quad (\text{A4})$$

In the A-series models $\bar{h} = h$, so that

$$\Delta = 2h, \quad s = 0, \quad (\text{A5})$$

while in non-diagonal invariants the left and right Kac labels may differ, giving nonzero spin.

A special property of Virasoro minimal models is that their spectrum contains only finitely many Virasoro primary operators. Therefore, in principle using exact Virasoro conformal blocks we could solve (3) exactly. In practice, however, there is still error due to a numerical evaluation of the Virasoro blocks using finite recursion iterations.

Following [17] we calculate the Virasoro blocks

$$\mathcal{V}(z, c, h_{\text{ext}}, h, N) = (16q)^{h - \frac{c-1}{24}} z^{\frac{c-1}{24} - 2h_{\text{ext}}} (1-z)^{\frac{c-1}{24} - 2h_{\text{ext}}} \theta_3(q)^{\frac{c-1}{2} - 16h_{\text{ext}}} \sum_{j=0}^{\lfloor N/2 \rfloor} q^{2j} H(c, h_{\text{ext}}, h_{\text{ext}}, h, N), \quad (\text{A6})$$

as truncated series in

$$q(z) = \exp\left[-\pi \frac{K(1-z)}{K(z)}\right], \quad (\text{A7})$$

where K is the complete elliptic integral of the first kind:

$$K(k) = \int_0^{\frac{\pi}{2}} \frac{d\varphi}{\sqrt{1 - k^2 \sin^2 \varphi}}. \quad (\text{A8})$$

$g_{\Delta_k, s_k}^{\Delta_\phi}(z, \bar{z})$ in (2) can be expressed as

$$g_{\Delta_k, s_k}^{\Delta_\phi}(z, \bar{z}) = \mathcal{V}(z, c, h_{\text{ext}}, h_k, N) \mathcal{V}(\bar{z}, c, h_{\text{ext}}, h_k, N), \quad (\text{A9})$$

therefore our non-linear search variables are c , h_{ext} and $\{h_k\}$.

Appendix B: Selection of minimal models and comparison with search results

In order to check the robustness of our method, we need to have many minimal models' spectrum as Fig. 2 shown. Minimal model fusion rule

$$\phi_{r_1, s_1} \times \phi_{r_2, s_2} = \sum_{r=|r_1-r_2|+1}^{\min(r_1+r_2-1, 2q-r_1-r_2-1)} \sum_{s=|s_1-s_2|+1}^{\min(s_1+s_2-1, 2p-s_1-s_2-1)} \phi_{r,s} \quad (\text{B1})$$

By fusion rule, we then have spectrum for any given (p, q, r, s) . The procedure of the minimal model spectrum computation will be the following. (1) Set a max p . (2) Scan through all possible $(p, q) \rightarrow$ Compute central charge. (3) Scan through all possible $(r, s) \rightarrow$ Compute external operator's conformal weight. (4) Get all internal operators' conformal weight by fusion rule.

In the following Table V, we present examples of best rewards for four-state search in the region of table III, where known five states models are available. In Table VI, we show a six state search in a five state region, neglecting the

ID	Spectrum	$h_{\text{int},0}$	$h_{\text{int},1}$	$h_{\text{int},2}$	$h_{\text{int},3}$	c	h_{ext}
1	Nearest MM	0.286462	0.372881	1.913580	3.113622	0.140625	0.928411
	Found	0.287020	0.372803	1.914932	3.116666	0.140634	0.929349
	Relative error	0.19%	-0.020%	0.070%	0.097%	-0.0064%	-0.10%
2	Nearest MM	0.251819	0.405152	1.846667	2.945152	0.244553	0.873599
	Found	0.252044	0.405123	1.847260	2.947820	0.244576	0.873992
	Relative error	0.089%	-0.0071%	0.032%	0.090%	-0.0094%	-0.044%
3	Nearest MM	0.283247	0.375758	1.907489	3.098225	0.150270	0.923398
	Found	0.283745	0.375704	1.908713	3.101137	0.150278	0.924243
	Relative error	0.17%	-0.014%	0.064%	0.093%	-0.0053%	-0.091%
4	Nearest MM	0.258874	0.398340	1.860534	2.979943	0.223387	0.884912
	Found	0.259215	0.398285	1.861406	2.983111	0.223426	0.885496
	Relative error	0.13%	-0.013%	0.046%	0.10%	-0.017%	-0.066%
5	Nearest MM	0.277270	0.381166	1.896104	3.069478	0.168201	0.914041
	Found	0.277816	0.381065	1.897435	3.072840	0.168233	0.914957
	Relative error	0.19%	-0.026%	0.070%	0.10%	-0.019%	-0.10%

TABLE V: Nearest Minimal Model (MM) vs. Found Spectrum

final state which has near zero OPE coefficient, we find that it recovers the five state solution.

Spectrum	$h_{\text{int},0}$	$h_{\text{int},1}$	$h_{\text{int},2}$	$h_{\text{int},3}$	$h_{\text{int},4}$	$h_{\text{int},5}$	c	h_{ext}
Five-state MM	0.2892	0.3704	1.9187	3.1267	6.7562	—	0.1324	0.9327
	Five-state Found	0.2892	0.3705	1.9187	3.1266	6.7568	—	0.1325
	Relative error	-0.0107%	0.0074%	-0.0031%	-0.0047%	0.0087%	—	0.0629% -0.0052%
Six-state Found	0.2873	0.3721	1.9151	3.1175	6.7440	7.5403	0.1382	0.9297
	Relative error	-0.66%	0.45%	-0.19%	-0.29%	-0.18%	—	4.37% -0.32 %

TABLE VI: Comparison of minimal model spectrum vs. the best reward five-state and six-state searches, including relative errors. The predicted OPE coefficient of the last state in the six state search is $\text{OPE} \pm \sigma = -1.203 \times 10^{-8} \pm 6.974 \times 10^{-9}$.

Appendix C: Specs of search

Covariance Matrix Adaptation Evolution Strategy (CMA-ES) is a stochastic, derivative-free algorithm for continuous, noisy black-box optimization. It works by evolving an initial random distribution of points toward regions of better rewards.

More concretely, CMA-ES maintains a multivariate normal search distribution

$$x \sim \mathcal{N}(\mu, \sigma^2 \mathcal{C}), \quad (\text{C1})$$

where μ is the mean (current best guess), σ is a global step size, and \mathcal{C} is a positive-definite covariance matrix. At each round (or epoch), several candidate solutions are drawn from this distribution, say N_c of them. They are then ranked according to their rewards from top to bottom. The mean μ is updated to a weighted average of the best candidates, the step size σ is updated depending on whether progress appears steady, and the covariance \mathcal{C} is reshaped so that it stretches along directions that repeatedly led to good solutions and squeezes along directions that performed poorly. This loop repeats until σ becomes very small or the improvements stall according to some stopping criterion.

The complete setup includes two parts: CMA-ES and the evaluation of the reward, that is, (9). However, there are two difficulties in evaluating this reward. First, we need to take large enough N_z to reduce the statistical noise. Second, multiple evaluations of the Virasoro block is required and thus is expensive. Hence, we evaluate the reward on

the GPU. Also, to reduce the overhead due to data transfer between GPU memory to RAM, we choose to implement CMA-ES on GPU.

To put CMA-ES on the GPU, we adopt the solver from *Evotorch*. In particular, we use the one in *evotorch.algorithms.CMAES*, which wraps the one in *pycma* so that it can be executed on the GPU backend. For the evaluation of the reward, we can parallelize the computation across N_c , N_z and N internal states. That is, during each epoch, we have N_c candidates, each of which has $N_z \times N$ components in $G_{k,j}$ in (5), and we calculate these $N_c \times N_z \times N$ terms with a single pass through the GPU. Hence, we can significantly reduce the runtime.

Since CMA-ES is a self-adaptive method, it is almost parameter-free once we set the initial conditions (to start the search) and stopping condition (to prevent time waste). In fact, we only need to choose (1) an initial step size σ_0 reflecting the scale of the search space, (2) the population size N_p , (3) the maximum number of steps for evolution (also known as generation) N_g , and (4) the tolerance t_σ to accept a solution when σ is below this value. The initial mean μ_0 is random sampled from the search space while the covariance matrix \mathcal{C} is initialized to identity. The code and the setting we use to run the search are provided in [18].

In our case, we run the code [18] on a single Nvidia A5500. As mentioned previously, for each epoch, the runtime is only a single pass on the GPU as long as there are enough threads for the computation. In our experience, GPU threads on A5500 are not exhausted when we calculate with up to $(N_c, N_z, N) = (500, 400, 5)$. In such case, with the level of recursion for Virasoro block evaluation being 40, the runtime is about 2 hours to search for 1000 points. As long as we have sufficient number of GPU threads, the runtime does not scale with N_c , N_z and N , and scale linearly with the recursion level and number of points to search.

Appendix D: Procedure of error analysis

As mentioned in Sec. II, we are focusing on the crossing symmetry of four-point functions with identical scalars. After decomposing it using conformal blocks, we parametrize our search space into $(\mathbf{h}_{int}, h_{ext}, c)$, in which we can plot known theories, such as minimal models, to qualify our search results. When theories are plotted in this space, they in general clustered into multiple lines in the space, see any figures in the main text. That makes the quantification of search results using errors from known theories ambiguous, since there's often another nearby theory. Hence, in this appendix, we explain how we perform error analysis and quantify how good the algorithm, CMA-ES, performs.

To calculate the error of a search result (a point in space), a straightforward way is to simply calculate the Euclidean distances between the result and all known theories, and then select the shortest one as the final prediction. However, we know that h_{ext} defines the boundary condition of a process and the central charge c classifies CFTs, which make them different roles from \mathbf{h}_{int} . Hence, in our procedure, we first make sure the search result has similar h_{ext} and c , and then calculate error in the full space. With this in mind, the following is the detail on how we calculate the error that qualifies our search results.

To determine which known minimal model is the closest to a given search result, we proceed as following. First, we apply a filter based on the relative errors in c , h_{ext} : Only minimal models whose deviations in both quantities are less than 5% remain as candidates, that is,

$$\frac{\|\mathbf{v} - \mathbf{v}_{mm}\|_2}{\|\mathbf{v}\|_2} < 5\% \quad (\text{D1})$$

where $\mathbf{v} = (h_{ext}, c)$, mm means the analytic values of minimal models, and we use L2 norm for the calculation.

Among the remaining candidates, we then compute the relative error in the full $(\mathbf{h}_{int}, h_{ext}, c)$ space and select the one with smallest error as the closest minimal model. More explicitly, the relative error is defined as

$$\min_i \left\{ \frac{\|\mathbf{u}_i - \mathbf{u}_{mm}\|_2}{\|\mathbf{u}_i\|_2} \right\} \quad (\text{D2})$$

where $\mathbf{u} = (\mathbf{h}_{int}, h_{ext}, c)$, and i labels the remaining candidates.

Appendix E: Further results

[3] D. Poland, S. Rychkov, and A. Vichi, *Rev. Mod. Phys.* **91**, 015002 (2019).

[4] S. El-Showk, M. F. Paulos, D. Poland, S. Rychkov, D. Simmons-Duffin, and A. Vichi, *Phys. Rev. D* **86**, 025022 (2012).

[5] S. El-Showk, M. F. Paulos, D. Poland, S. Rychkov, D. Simmons-Duffin, and A. Vichi, *J. Stat. Phys.* **157**, 869 (2014), arXiv:1403.4545 [hep-th].

[6] F. Kos, D. Poland, D. Simmons-Duffin, and A. Vichi, *JHEP* **11**, 106 (2015), arXiv:1504.07997 [hep-th].

[7] A. A. Belavin, A. M. Polyakov, and A. B. Zamolodchikov, *Nucl. Phys. B* **241**, 333 (1984).

[8] A. Laio, U. L. Valenzuela, and M. Serone, *Phys. Rev. D* **106**, 025019 (2022), arXiv:2206.05193 [hep-th].

[9] G. Kántor, V. Niarchos, and C. Papageorgakis, *Phys. Rev. Lett.* **128**, 041601 (2022), arXiv:2108.08859 [hep-th].

[10] G. Kántor, V. Niarchos, and C. Papageorgakis, *Physical Review D* **105** (2022), 10.1103/physrevd.105.025018.

[11] G. Kántor, V. Niarchos, C. Papageorgakis, and P. Richmond, *Phys. Rev. D* **107**, 025005 (2023), arXiv:2209.02801 [hep-th].

[12] N. Hansen, arXiv preprint arXiv:1604.00772 (2016).

[13] A. Belavin, A. Polyakov, and A. Zamolodchikov, *Nuclear Physics B* **241**, 333 (1984).

[14] F. A. Dolan and H. Osborn, *Nucl. Phys. B* **599**, 459 (2001), arXiv:hep-th/0011040.

[15] D. Pappadopulo, S. Rychkov, J. Espin, and R. Rattazzi, *Phys. Rev. D* **86**, 105043 (2012), arXiv:1208.6449 [hep-th].

[16] G. C. R. Douglas C. Montgomery, *Applied Statistics and Probability for Engineers*, 7th Edition (Wiley, 2018).

[17] H. Chen, C. Hussong, J. Kaplan, and D. Li, *Journal of High Energy Physics* **2017** (2017), 10.1007/jhep09(2017)102.

[18] Github link to our implementation (2025).

[19] D. Simmons-Duffin, *JHEP* **03**, 086 (2017), arXiv:1612.08471 [hep-th].

[20] Y. Kusuki, *JHEP* **01**, 025 (2019), arXiv:1810.01335 [hep-th].

[21] G. Shala, A. Biedenkapp, N. Awad, S. Adriaensen, M. Lindauer, and F. Hutter, in *Parallel Problem Solving from Nature – PPSN XVI*, Lecture Notes in Computer Science, Vol. 12269 (Springer, Cham, 2020) pp. 691–706.

[22] T. V. Vishnu, P. Malhotra, J. Narwariya, L. Vig, and G. Shroff, arXiv e-prints , arXiv:1907.06901 (2019), arXiv:1907.06901 [cs.LG].

[23] R. T. Lange, T. Schaul, Y. Chen, T. Zahavy, V. Dallibard, C. Lu, S. Singh, and S. Flennerhag, in *Proceedings of the International Conference on Learning Representations (ICLR)* (2023) arXiv:2211.11260.

[24] T. Chen, X. Chen, W. Chen, H. Heaton, J. Liu, Z. Wang, and W. Yin, *Journal of Machine Learning Research* **23**, 1 (2022).

[25] K. Li and J. Malik, arXiv e-prints , arXiv:1606.01885 (2016), arXiv:1606.01885 [cs.LG].

[26] A. Strominger, *JHEP* **10**, 034 (2001), arXiv:hep-th/0106113.

[27] D. Poland, V. Prilepsina, and P. Tadić, *JHEP* **10**, 153 (2023), arXiv:2305.08914 [hep-th].

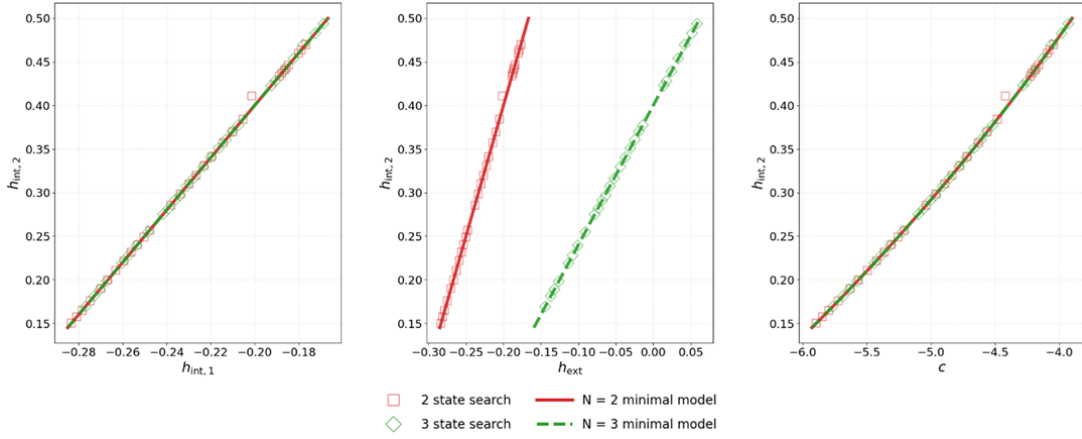


FIG. 5: Search results around Yang-Lee CFT region with 2 and 3 internal operators in projection to $(O, h_{int,2})$ where $O \in \{h_{int,1}, h_{ext}, c\}$. The line of minimal model represents minimal models with $p, q \leq 200$.

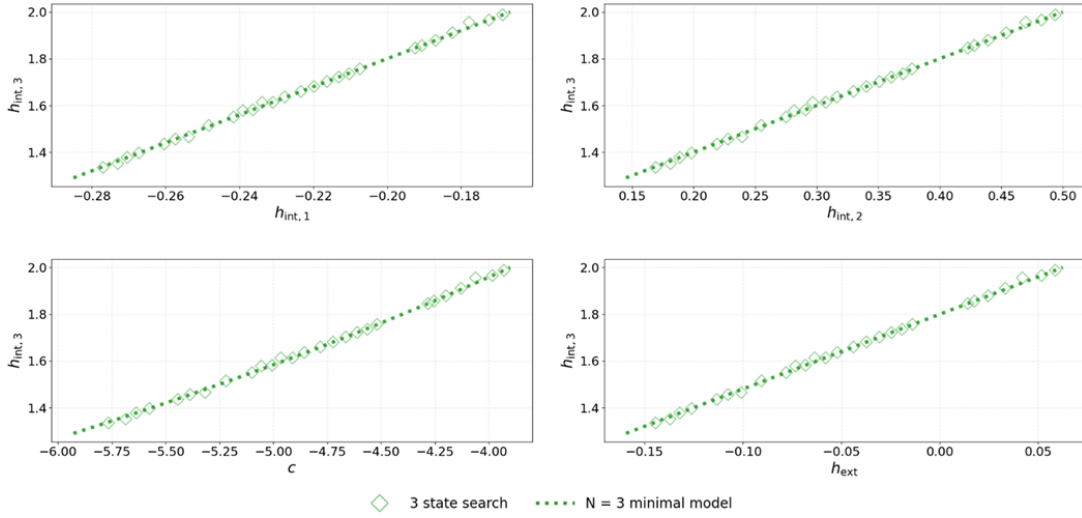


FIG. 6: Search results around Yang-Lee CFT region with 3 internal operators in projection to $(O, h_{int,3})$ where $O \in \{h_{int,1}, h_{int,2}, h_{ext}, c\}$. The line of minimal model represents minimal models with $p, q \leq 200$.